Chapter VI

CRITICAL PHYSICAL INGREDIENTS FOR DYNAMOS: TURBULENCE AND INSTABILITIES

Astrophysical MHD turbulence: confluence of observations, simulations, and theory

Blakesley Burkhart[1] and Alex Lazarian[1]

[1] Astronomy Department, University of Wisconsin, Madison, 475 N. Charter St., WI 53711, USA

Abstract. Magnetohydrodynamic (MHD) turbulence is a critical component of the current paradigms of star formation, dynamo theory, particle transport, magnetic reconnection and evolution of the ISM. In order to gain understanding of how MHD turbulence regulates processes in the Galaxy, a confluence of numerics, observations and theory must be imployed. In these proceedings we review recent progress that has been made on the connections between theoretical, numerical, and observational understanding of MHD turbulence as it applies to both the neutral and ionized interstellar medium.

Keywords. Turbulence ,MHD (magnetohydrodynamics), ISM: general

1. Introduction

It is now generally accepted that turbulence is one of the major processes that governs the structure formation and evolution of different phases of the interstellar medium (Elmegreen & Scalo 2004) and is critically important for many astrophysical processes such as magnetic reconnection, cosmic ray acceleration, and heat transport. The evidence for the role of turbulence in the diffuse and molecular ISM is overwhelming. Some of the most famous studies include: the "big power law" of the electron density fluctuations (Armstrong *et al.* 1995; Chepurnov & Lazarian 2010), fractal structure in the molecular media (Stutzki *et al.* 1998), and intensity fluctuations contributed by both density and turbulent velocity in channel maps (Crovisier & Dickey 1983).

In addition to being turbulent, astrophysical plasmas are magnetized. The magnetization of astrophysical fluids most frequently arises from the dynamo action to which turbulence is an essential component (see Schekochihin *et al.* 2007). In fact, it has been shown that turbulence converts (in weakly magnetized conducting fluid) from five to ten percent of the energy of the cascade into the magnetic field energy (see Cho *et al.* 2009). This fraction *does not* depend on the original magnetization† and therefore magnetic fields will come to equipartition‡ with the turbulent motions within a few eddy turnover times.

Despite the importance of MHD turbulence for the solar wind, ISM and IGM, finding ways to quantify and study it still vexes researchers. This is because astrophysical MHD turbulence is a complex nonlinear phenomena that can occur in a multiphase media with many energy injection sources. Due to this complexity, numerical simulations have become increasingly vital to the study of the ISM. Although numerical simulations have made gains in terms of both resolution and ability to simulate the wide range of physics found in the ISM such as shocks, two phase fluids, instabilities, magnetic fields, and core

---

† This makes the problem of the initial or seed magnetic field, that for a long time has worried researchers, rather trivial. Very weak magnetic fields, e.g. generated by Bierman battery (see Lazarian 1992) can be amplified fast in a turbulent plasmas.

‡ In supersonic flows compressibility effects induce deviations from the equipartition.
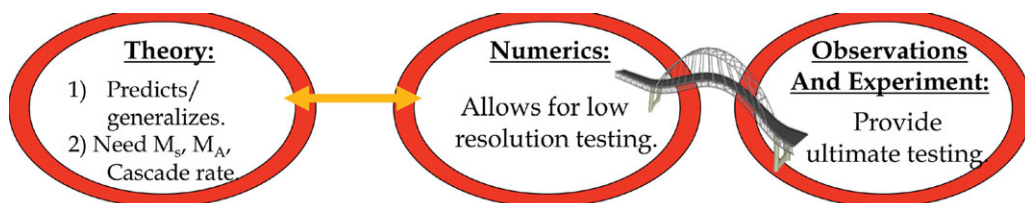
Figure 1. The synergetic approach for studying turbulence in the ISM. Theoretical studies (as outlined in Section 3) provide predictions for scaling laws which can be tested in a low resolution setting with numerical simulations. Numerical simulations can then be made into synthetic observations and compared with the real observations of the ISM (as outlined in Section 4). At this stage, theory again provides information on the expected behavior of the turbulence.

collapse, simulations still are not able to reach the Reynolds numbers (i.e. the ratio of the viscous time scale to eddy turn over time scale) and dynamical range that is seen in the ISM. This is because the number of floating-point operations required scales as R_e^3. The Reynolds numbers are typically very large in astrophysical flows as the scales are large. As magnetic fields decrease the viscosity for the plasma motion perpendicular to their direction, Re numbers become astronomically large. For instance, Re numbers of 10^{10} are very common for astrophysical flows.

Despite their limitations, numerical simulations of turbulence still provide one of the best avenues for researchers of the ISM to understand the nature of magnetized turbulence. The combined efforts of predictive theory and numerical tests have greatly increased our knowledge of MHD turbulence, including its anisotropy, intermittency, and imbalanced nature (see Cho & Lazarian 2003; Kowal *et al.* 2007; Beresnyak & Lazarian 2010). One of the main approaches for characterizing ISM turbulence in both numerical simulations and from observations is based on using statistical techniques and descriptions. The most common "go-to" tool for both observers and theorists alike is the spatial power spectrum. This is because the power spectrum provides valuable information on the nature of the turbulent cascade including information about the injection scale, inertial range, and dissipation range of turbulence. While the power spectrum gives information about the energy per wavenumber (or frequency), it only contains the Fourier amplitudes and completely ignores the phases. Furthermore, the power-spectrum is fairly insensitive to the influence of the magnetic field, while other statistics (such as higher order spectra and structure functions) show large dependencies on the magnetic pressure. These issues provide motivation for the development of techniques that can be complementary to the power spectrum for studies of turbulence.

In these proceedings we briefly summarize what we feel is the most constructive methodology for studying MHD Turbulence in astrophysical settings. We advocate for a synergetic use of statistical tools applied to both observations and synthetic numerical simulations which take into account the appropriate physics necessary for comparison. We organize these proceedings as follows: In §2 we describe our approach for the confluence of observations and numerical simulations regarding studies of MHD turbulence. In §3 we review the current theoretical description of MHD turbulence that is appropriate for the ISM. In §4 we discuss progress that has been made in regards to studying turbulence in the neutral and ionized phases of the ISM along with statistics for studying the magnetic field. In §5 we make our concluding remarks and summarize.

Turbulence Statistics: The Bridge Between Numerics and Observations
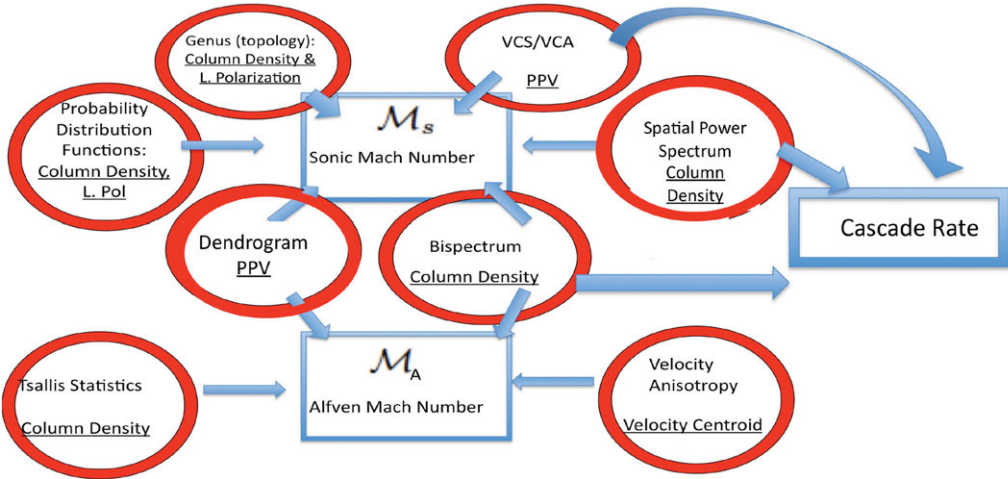
Figure 2. Illustration highlighting different statistical tools capable of providing information about the sonic and Alfvénic Mach numbers and the injection scale. These are the critical parameters to explore when discussing MHD turbulence in the interstellar medium.

2. How to Study MHD Turbulence in the ISM

In general, the best strategy for studying a difficult subject like interstellar turbulence is to use a synergetic approach, combining theoretical knowledge, numerical simulations, and observational data via statistical studies. In this way one can obtain the most complete and reliable picture of the physics of turbulence.

There has been substantial progress in the development of techniques to study turbulence in the last decade. Techniques for the study of turbulence can be tested empirically using parameter studies of numerical simulations or with the aid of analytical predictions. The parameters to be varied (see Burkhart & Lazarian 2011) include the Reynolds number, sonic and Alfvénic Mach number, injection scale, equation of state, and, for studies of molecular clouds, should include radiative transfer and self-gravity (see Ossenkopf 2002; Padoan *et al.* 2003; Goodman *et al.* 2009). The sonic Mach number is the dimensionless ratio of the flow velocity to the sound speed, i.e. $M_s \equiv \langle V_L/c_s \rangle$. The Alfvén number is the dimensionless ratio of the flow velocity to the Alfvén speed, i.e. $M_A \equiv \langle V_L/v_A \rangle$, where $V_L = v_{\rm rms}$ is the turbulent velocity at the injection scale. As the Alfvén speed depends on the magnetic field, this ratio can provide information on the strength of the magnetic field relative to the velocity and density.

As we will show in Section 3, the minimal information needed in order to obtain a picture of the local cascade of MHD turbulence is the compressibility (sonic Mach number), magnetization (Alfénic Mach number) and cascade rate (given by the spectrum). Some recently developed techniques that probe these parameters include the application of probability distribution functions (PDFs), wavelets, spectral correlation function (SCF), delta-variance, the principal component analysis, higher order moments, Genus, Tsallis statistics, spectrum and bispectrum (Gill & Henriksen 1990; Stutzki *et al.* 1998; Rosolowsky *et al.* 1999; Brunt & Heyer 2002; Kowal, Lazarian & Beresnyak 2007; Chepurnov *et al.* 2008; Burkhart *et al.* 2009; Esquivel & Lazarian 2010; Toffelmire *et al.* 2011). Additionally, these techniques are being tested and applied to different wavelengths and

types of data. We outline some of these techniques and their dependency on the sonic and Alfvénic Mach numbers and the turbulent cascade in Figure 2.

3. Theoretical Description of MHD Turbulence

The drivers of turbulence, e.g. supernovae explosions in the interstellar medium, inject energy at large scales and then the energy cascades down to small scales through the hierarchy of eddies. The famous Kolmogorov picture (Kolmogorov 1941) corresponds to hydrodynamic turbulence, but as we discuss further, a qualitatively similar picture of turbulence also develops in magnetized fluids/plasmas.

3.1. *Kolmogorov 1941*

The hydrodynamic counterpart of the MHD turbulence theory is the famous Kolmogorov (1941) theory of turbulence. Here energy is injected at large scales, creating large eddies which correspond to large Re numbers and therefore do not dissipate energy through viscosity† but transfer energy to smaller eddies. The process continues until the cascade reaches the eddies that are small enough to dissipate energy over eddy turnover time. In the absence of compressibility the hydrodynamic cascade of energy is $\sim v_l^2/\tau_{casc,l} = const$, where v_l is the velocity at the scale l and the cascading time for the eddies of size l is $\tau_{cask,l} \approx l/v_l$. From this the well known relation $v_l \sim l^{1/3}$ follows.

3.2. *Strong and Weak Alfvénic turbulence*

The ISM is both turbulent and magnetized, and therefore Alfvénic perturbations are vital. Numerical studies in Cho & Lazarian (2002, 2003) showed that Alfvénic turbulence develops an independent cascade which is marginally affected by the fluid compressibility. This observation corresponds to theoretical expectations of the Goldreich & Sridhar (1995, henceforth GS95) theory that we briefly describe below.

A frequent mental picture that astrophysicists have of the Alfvénic turbulence is based on Alfvén waves with wavevectors along the magnetic field. This is not true for the strong Alfvénic turbulence which, similar to its hydrodynamic counterpart, can be described in terms of eddies‡. However, contrary to Kolmogorov turbulence, in the presence of dynamically important magnetic field eddies become anisotropic. At the same time, one can imagine eddies mixing magnetic field lines perpendicular to the direction of magnetic field. For the latter eddies the original Kolmogorov treatment is applicable resulting in perpendicular motions scaling as $v_l \sim l_\perp^{1/3}$, where $l_\perp$ denotes eddy scales measured perpendicular to magnetic field. These mixing motions induce Alfvénic perturbations that determine the parallel size of the magnetized eddy. The key stone of the GS95 theory is *critical balance*, i.e. the equality of the eddy turnover time $l_\perp/v_l$ and the period of the corresponding Alfvén wave $\sim l_\parallel/V_A$, where $l_\parallel$ is the parallel eddy scale and V_A is the Alfvén velocity. Making use of the earlier expression for v_l one can easily obtain $l_\parallel \sim l_\perp^{2/3}$, which reflects the tendency of eddies to become more and more elongated as the energy cascades to smaller scales (see Beresnyak, Lazarian & Cho 2005).

---

† Reynolds number $Re \equiv L_f V/\nu = (V/L_f)/(\nu/L_f^2)$ which is the ratio of an eddy turnover rate $\tau_{eddy}^{-1} = V/L_f$ and the viscous dissipation rate $\tau_{dis}^{-1} = \eta/L_f^2$. Therefore large Re correspond to negligible viscous dissipation of large eddies over the cascading time τ_{casc} which is equal to τ_{eddy} in Kolmogorov turbulence.

‡ The description in terms of interacting wavepackets or modes is also possible with the corresponding wavevectors tending to get more and more perpendicular to the magnetic field as the cascade develops.

Table 1
Regimes and ranges of MHD turbulence

Type of MHD turbulence	Injection velocity	Range of scales	Motion type	Ways of study
Weak	$V_L < V_A$	$[L, l_{trans}]$	wave-like	analytical
Strong subAlfvenic	$V_L < V_A$	$[l_{trans}, l_{min}]$	eddy-like	numerical
Strong superAlfvenic	$V_L > V_A$	$[l_A, l_{min}]$	eddy-like	numerical

L and l_{min} are injection and dissipation scales
l_{trans} and l_A are given by Eq. (3.2) and Eq. (3.1), respectively.

It is important to stress that the scales $l_\perp$ and $l_\parallel$ are measured in respect to the system of reference related to the direction of the local magnetic field "seen" by the eddy. In terms of mixing motions, it is rather obvious that the free Kolmogorov-type mixing is possible only in respect to the local magnetic field of the eddy rather than the mean magnetic field of the flow.

GS95 theory assumes the isotropic injection of energy at scale L and the injection velocity equal to the Alfvén velocity in the fluid V_A, i.e. the Alfvén Mach number $M_A \equiv (V_L/V_A) = 1$, where V_L is the injection velocity. Thus it provides the description of trans-Alfvénic turbulence. This model was later generalized for both sub-Alfvénic, i.e. $M_A < 1$, and super-Alfvénic, i.e. $M_A > 1$, cases (see Lazarian & Vishniac 1999 and Lazarian 2006, respectively; see also Table 1). Indeed, if $M_A > 1$, instead of the driving scale L for one can use another scale, namely l_A:

$$l_A = L(V_A/V_L)^3 = LM_A^{-3} \tag{3.1}$$

which is the scale at which the turbulent velocity equals to V_A. For $M_A \gg 1$ magnetic fields are not dynamically important at the largest scales and the turbulence at those scales follows the isotropic Kolmogorov cascade $v_l \sim l^{1/3}$ over the range of scales $[L, l_A]$. At the same time, if $M_A < 1$, the turbulence obeys GS95 scaling (also called "strong" MHD turbulence) not from the scale L, but from a smaller scale l_{trans} given by:

$$l_{trans} \sim L(V_L/V_A)^2 \equiv LM_A^2 \tag{3.2}$$

While in the range $[L, l_{trans}]$ the turbulence is "weak".

One also should keep in mind that the notion "strong" should not be associated with the amplitude of turbulent motions but only with the strength of the non-linear interaction. As the weak turbulence evolves, the interactions of wave packets *get stronger* making the turbulence strong. In this case, the amplitude of the perturbations can be very small.

4. Comparison with Observations

4.1. *Diagnostics of Neutral Phase Turbulence: Velocity and Density Spectrum*

There have been many works over the last ten years which study the density/velocity power spectrum in radio PPV cubes of neutral hydrogen in both the Galaxy and Magellanic clouds in the context of turbulence (see Crovisier & Dickey 1983; Stanimirovic *et al.* 1999; Stanimirovic & Lazarian 2001; Burkhart *et al.* 2010 and references therein). The slope of the power spectrum not only gives information on the cascading rate but

it is known to depend on the sonic Mach number (see Figure 2). Here we briefly outline application of the spatial column density power spectrum to the Small Magellanic Cloud (SMC, see Burkhart *et al.* 2010) and the application of the velocity coordinate spectrum technique (VCS) to high latitude HI emission from the GALFA survey (see Chepurnov *et al.* 2010). Both of these studies are particularly interesting in the context of these proceedings as they connect the observations with numerical simulations and theoretical predictions, rather then just blindingly applying the power spectrum to the data.

4.1.1. *The Small Magellanic Cloud*

Stanimirovic & Lazarian (2001) estimated the power-law slope of -3.3 for the spatial power spectrum of the HI column density image of the SMC. Burkhart *et al.* 2010 measure the power spectrum slope for simulated column density maps with varying sonic and Alfvénic Mach numbers and compared the resulting power law slopes with the SMC slope. Figure 3 shows how the power spectral slope changes with the sonic Mach number in the simulations, while the straight line denoting the results for the SMC. The slope is increasingly shallow for supersonic models and levels off for very high Mach number turbulence. This is expected as higher Mach number turbulence has more density irregularities and more power on small scales.
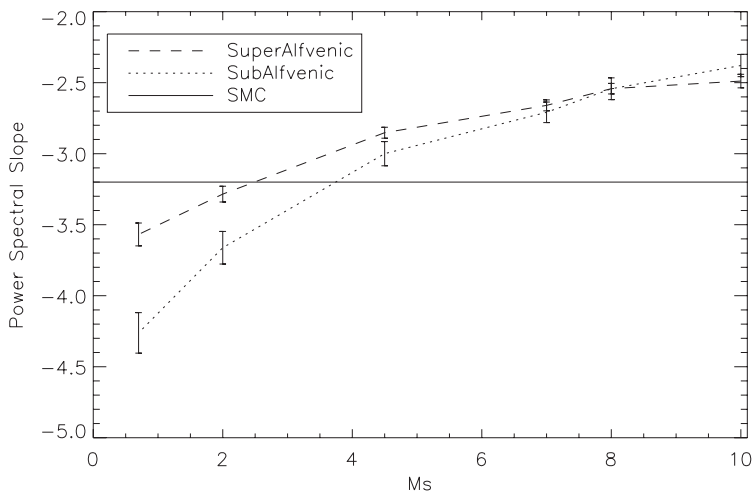

Figure 3. Power spectral slope vs. sonic Mach number for a sub-Alfvénic ($\mathcal{M}_A = 2.0$, dotted line) and a super-Alfvénic ($\mathcal{M}_A = 0.7$, dashed line) simulation. The spectral slope of the SMC (-3.3) is shown as a straight line.

Burkhart *et al.* 2010 found via the analysis of the column density power spectrum that the SMC was supersonic with Mach numbers ranging from $\mathcal{M}_s \approx 2.0 - \mathcal{M}_s \approx 4.0$. They then compared these Mach numbers with those derived from a *purely observational method* which utilizes information on spin temperature (derived from absorption lines) and the kinetic temperature (derived from the FWHM of HI emission). The resulting cold gas Mach number histogram peaked at $\mathcal{M}_s = 3.5 - 4$, which is in agreement with the range found from the spectral slope analysis derived from numerical simulations.

4.1.2. *Galactic High Latitude HI*

The spatial column density spectrum is limited for studies of the turbulence spectra, as it does not contain any information on velocity. Fortunately, several statistics have been developed to study the power spectrum of velocity from the observations. These
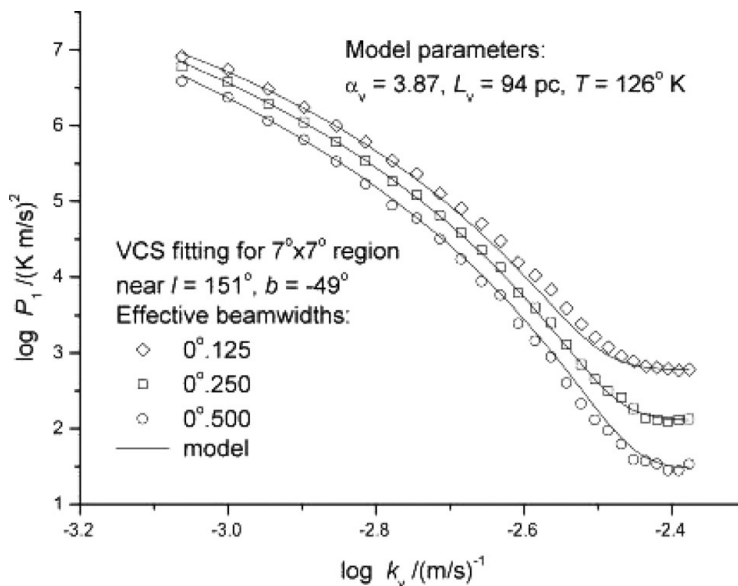
Figure 4. Fitting of turbulent models and observational data for different resolutions. Application of the VCS high latitude HI Arecibo data. The spatial resolution of the maps was decreased to illustrate the VCS in both high and low resolution regimes. ϵ here is the power spectrum index, which for the Kolmogorov turbulence is 11/3. The measured ϵ is in the range $[3.52; 3.57]$. The energy injection scale is 94 pc.

include the Velocity Coordinate Spectrum (VCS, see Lazarian & Pogosyan 2006), Velocity Channel Analysis (VCA, Lazarian & Pogosyan 2004), and velocity centroids (Esquivel & Lazarian 2005, only for subsonic turbulence).

Chepurnov *et al.* 2010 presented a first taste of the power of the VCS technique on high latitude HI data via the GALFA survey (see Peek *et al.* 2011). Figure 4 shows the results of their VCS-analysis of galactic high latitude data. Rather than first correcting for the gas thermal broadening, then fitting the power law into the VCS spectrum as discussed in Lazarian & Pogosyan (2006), they used analytical expressions to find the model (which depends on the gas temperature, injection scale of the turbulence and turbulent energy) that fits the data set corresponding to VCS for data at different spatial resolutions. The resolutions play for the VCS a similar† role as the thickness of slices Δv for the VCA and therefore PPV data cubes at different resolutions are non-trivially related, as far as the VCS analysis is concerned.

Fitting data to the models opens ways of studying non-power law turbulence, e.g. turbulence at the injection or dissipation scales. It also allows for studies of turbulence when thermal broadening is important. The results in Figure 4 show that the model of turbulence with spectrum steeper than Kolmogorov, i.e. with $E_v \sim k^{-1.9}$, the temperature of the cold gas around 130K and a single injection scale of 100pc (corresponding to the scale of supernova). The fact that the temperature of the gas, the injection scale and turbulent energy can be recovered via the VCS is very encouraging for studies of turbulence, as these parameters are critical to many astrophysical motivated issues such as the star formation rate, heating in the ISM, and the galactic fountain.

† The important difference is that with VCS, we can restore the velocity spectrum for any resolution.
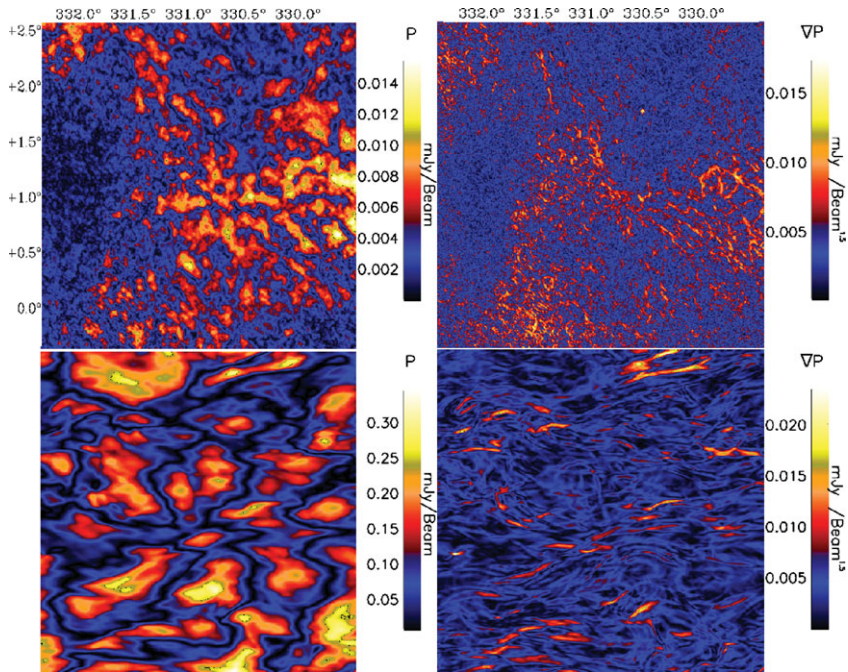
Figure 5. Top: Observational P (left) and $|\nabla\mathbf{P}|$ (right) from the SGPS data used in Gaensler *et al.* 2011. Bottom: Subsonic MHD simulation with P (left) and $|\nabla\mathbf{P}|$ (right).

4.2. *Diagnostics of Ionized Phase Turbulence: Polarization Gradients*

4.2.1. *Polarization Gradients*

Several authors have discussed the prospects of using radio polarization maps to study turbulence (see Gaensler *et al.* 2011, Burkhart, Lazarian & Gaensler 2012, and references therein). Faraday rotation maps of linearly polarized radio signals are especially promising as they provide very sensitive probes of fluctuations in magnetic field and ionized gas density. In these proceedings we highlight the use of polarization gradients to study ISM turbulence in the ionized phase of the ISM, although we would like to also draw attention to many other studies that employ PDFs of the emission measure to study turbulence in this phase (see Hill *et al.* 2008; Berkhuijsen & Fletcher 2008).

The use of spatial gradients to highlight small fluctuations seen in polarization maps was first discussed by Gaensler *et al.* (2011). When the spatial gradient is applied to maps of vector $\mathbf{P} = (Q, U)$ a complex web of filamentary structures is revealed. These filaments (see right column of Figure 5 for an example) were interpreted by Gaensler *et al.* (2011) and Burkhart, Lazarian, & Gaensler 2012 as rapid fluctuations in n_e and B along the LOS due to turbulence.

Maps of $|\nabla\mathbf{P}|$ change morphology and intensity as turbulence transitions from subsonic to supersonic. Burkhart, Lazarian, & Gaensler (2012) analyzed $|\nabla\mathbf{P}|$ maps from both observations and simulations using PDFs and a topology tool known as the Genus (see Figure 2). They found that one could quantify the sonic Mach number using a statistical analysis of the maps of $|\nabla\mathbf{P}|$.

4.2.2. *Extending the "Big Power Law" of Electron Density Fluctuations*

Perhaps one of the most famous early pieces of evidence for the turbulent ionized ISM was in the analysis of the spectrum of electron scintillation and scattering as provided
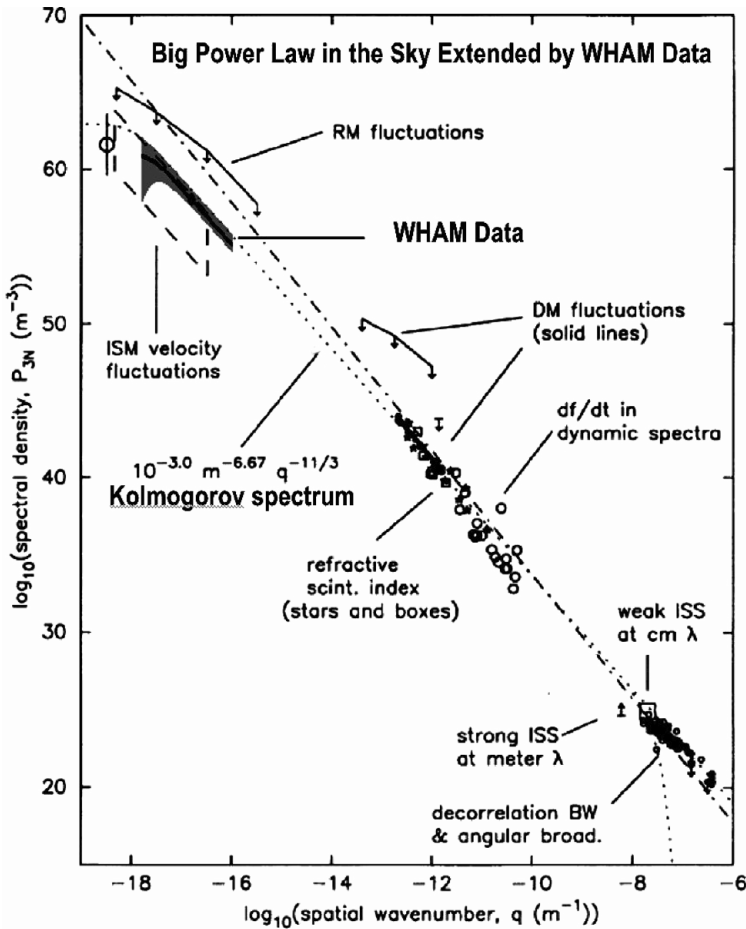
Figure 6. Turbulence in the interstellar gas as revealed by electron density fluctuations: "Big Power Law in the Sky" in Armstrong *et al.* (1995) extended using WHAM data. Modified from Chepurnov & Lazarian (2010).

by Armstrong *et al.* 1995. These results have recently been expanded upon using the Wisconsin H$_\alpha$ Mapper (WHAM) data on electron density fluctuations (Chepurnov & Lazarian 2010). Figure 6 shows the turbulent power density plotted against the inverse of the scale length, with data at large scales, i.e. at small wavenumbers q. The power law extends from pc scales down to AU scales.

4.3. *Diagnostics of the Magnetic Field*

One important point of GS95 (reviewed in Section 3) is that the mixing motions associated with Alfvénic turbulence induce scale-dependent anisotropy, which increase as the cascade progresses. The observed anisotropy is seen strongly in motions perpendicular to the field and increases with increasing magnetic field. This effect can be seen via analysis of structure functions of velocity centroid maps, which are available from radio observations and synthetic observations. Esquivel & Lazarian (2011, henceforth EL11) and Leão *et al.* (2012, in prep., henceforth LBLM12) applied structure functions to velocity centroid maps of synthetic observations and found that the observed anisotropy could be used to determine the strength of the perpendicular component of the magnetic field.
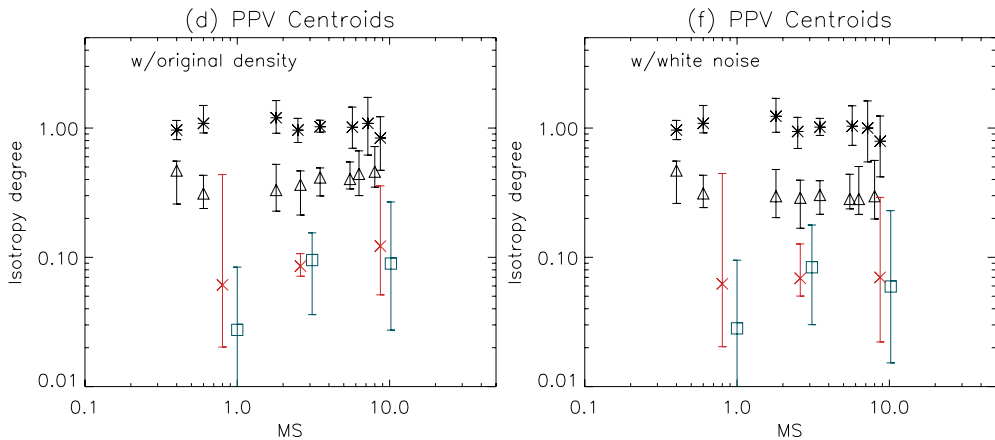
Figure 7. Degree of anisotropy in all the models averaged over scales from 10 grid points to 1/5 of the computational box. The left panel is for the unaltered PPV Centroid map and the right panel is for the PPV centroid map with Gaussian white noise added. The horizontal axis corresponds to the sonic Mach number, and the Alfvénic Mach number is indicated by the various symbols: x symbols for cases with $\mathcal{M}_A = 0.2$, squares represent cases with $\mathcal{M}_A = 0.3$, triangles for $\mathcal{M}_A = 0.7$, and asterix for $\mathcal{M}_A = 7.5$. In all panels the results are obtained by averaging the two cases where the LOS is perpendicular to the mean field. The error bars show the maximum variation of the averaging procedure (including variation across scales).

The method outlined in EL11 and LBLM12 is as follows: the structure function $(SF(\mathbf{r}) = \langle [f(\mathbf{x}) - f(\mathbf{x} + \mathbf{r})]^2 \rangle)$ of the velocity centroid maps is calculated and the degree of anisotropy is quantified by taking the ratio of the structure functions in two perpendicular directions to the LOS, usually intersecting the distribution center, as for example, $SF_{C,z}(x,0)/SF_{C,z}(0,y)$. The structure function is a two dimensional distribution that can be approximately circular for isotropic turbulence and elliptical for anisotropic turbulence (see EL11 and LBLM12 for details). When looking parallel to the mean magnetic field the degree of isotropy is nearly 100% while when looking perpendicular to the mean magnetic field the structures become increasingly anisotropic, as is expected from the predictions of the GS95 theory.

Fig. 7 shows a comparison of the isotropy degree as a function of $\mathcal{M}_s$ for synthetic observations with four different magnetic field strengths using velocity centroid maps created with both the original 3D density (left panel) and for density with Gaussian white noise added to further mimic the telescope resolution (right panel). It is clear that the degree of anisotropy depends mostly on the Alfvénic Mach number: as values of the magnetic field increase, the level of anisotropy increases. Centroid anisotropy also shows a weak dependence on $\mathcal{M}_s$, but only for moderate to low magnetizations. One can attribute such dependence to the original density field (i.e., arising from shocks in supersonic turbulence).

The dependence on the Alfvénic Mach number and a weak dependence on $\mathcal{M}_s$ shown in EL11 and LBLM12 are encouraging. While the sonic Mach number can be obtained by a variety of techniques (Kowal *et al.* 2007; Burkhart *et al.* 2009), the Alfvénic Mach number is not so straightforwardly obtained. With the use of the technique outlined here, along with others such as the Chandrasekhar-Fermi technique, (see, for instance, Falceta-Gonçalves *et al.* 2008) the Alfvénic Mach number can be quantified in the observational data.

5. Concluding Remarks

Observational studies of ISM turbulence are extremely important. The wealth of observational data currently available and coming to online due to the surveys, such as LOFAR, calls for techniques that can make use of this data in order to study turbulence that critically affects most astrophysical processes. From the observational data one would like to obtain the characteristics of turbulence, e.g. intensity of its driving, importance of magnetic eld in the dynamics of the media. In these proceedings we stressed that an *observational* understanding of MHD turbulence is best guided by the advances in numerical simulations (via the creation of synthetic observations) and theoretical predictions. We briefly reviewed the GS95 theory of MHD turbulence to show that the primary quantities needed to understand turbulence are the cascade rate, the sonic Mach number, and Alfvénic Mach number. Then we reviewed several works that derive these quantities via the use of newly developed statistic techniques that can be applied to both the neutral and ionized ISM.

The goal of such studies to to present a consistent picture of the turbulent ISM. That is, not to use just one statistical tool to obtain the desired parameters, but rather to use multiple tools simultaneously. Additional ways of studying turbulence are very valuable as the ISM is very complex. Furthermore, different measures are more sensitive to different phases of the ISM. This consistency of observations with numerical simulations and theory provides further evidence of the overwhelming importance of MHD turbulence in the ISM.

Acknowledgements

References

Armstrong, J. W., Rickett, B. J., & Spangler, S. R. 1995, *ApJ*, 443, 209
Beetz, C., Schwarz, C., Dreher, J., & Grauer, R. 2008, *Phys. Lett. A*, 372, 3037
Beresnyak, A. & Lazarian, A., 2010, *ApJL*, 722, L110
Beresnyak, A., Lazarian, A., & Cho, J. 2005, *ApJL*, 624, L93
Berkhuijsen, E., M. & Fletcher, A., 2008, *MNRAS*, 390, 19
Brunt, C. & Heyer, M. 2002, *ApJ*, 566, 27
Brunt, C. M., 2010, *A&A* 513, A67
Burkhart, B., Falceta-Gonçalves, D., Kowal, G., & Lazarian, A. 2009, *ApJ*, 693, 250
Burkhart, B., Stanimirovic, S., Lazarian, A., & Grzegorz, K., 2010, *ApJ*, 708, 1204
Burkhart, B. & Lazarian, A., 2011, *ASPC*, 44,9
Burkhart, B., Lazarian, A., & Gaensler, B., 2012, *ApJ*, 708, 1204
Burkhart, B. & Lazarian, A., 2012, *ApJ*, 755, 19
Chepurnov, A., Lazarian, A., Gordon, J., & Stanimirovic, S., 2008, *ApJ*, 688, 1021
Chepurnov, A. & Lazarian, A. 2010, *ApJ*, 710, 853
Chepurnov, A., Lazarian, A., Stanimirović, S., Heiles, C., & Peek, J. E. G., 2010, *ApJ*, 714, 1398
Cho, J. & Lazarian, A. 2002, *Phys. Rev. Lett.*, 88, 5001
Cho, J. & Lazarian, A. 2003, *MNRAS*, 345, 325
Cho, J., Vishniac, E. T., Beresnyak, A., Lazarian, A., & Ryu, D. 2009, *ApJ*, 693, 1449
Crovisier, J. & Dickey, J. M. 1983, *A&A*, 122, 282
Elmegreen, B. & Scalo, J., *ARA&A*, 42, 211 (2004)
Esquivel & Lazarian, 2005, *ApJ*,631,320

Esquivel, A. & Lazarian, A., 2010, *ApJ*, 710, 125

Esquivel, A. & Lazarian, A., 2011, *ApJ*, 740, 117 (EL11)

Falceta-Gonçalves, D., Lazarian, A., & Kowal, G., 2008, *ApJ*, 679, 537

Gaensler *et al.*, 2011, Nature, 478, 214

Gill, A. & Henriksen, R. N., *ApJ*, 365, L27 (1990)

Goldreich, P. & Sridhar, S. 1995, *ApJ*, 438, 763 (GS95)

Goodman, A. A., Pineda, J. E., & Schnee, S. L. 2009, *ApJ*, 692, 91

Hill *et al.*, 2008, *ApJ*, 686, 363

Kolmogorov, A. 1941, *Akademiia Nauk SSSR Doklady*, 30, 301

Kowal, G., Lazarian, A., & Beresnyak, A. 2007, *ApJ*, 658, 423

Lazarian, A. 1992, *AAP*, 264, 326

Lazarian, A. 2006, *ApJL*, 645, L25

Lazarian, A. & Pogosyan, D. 2006, *ApJ*, 652, 1348

Lazarian, A. & Pogosyan, D. 2004, *ApJ*, 616, 943

Lazarian, A. & Vishniac, E. 1999, *ApJ*, 517, 700 (LV99)

Leão, I., Burkhart, B., Lazarian, A., & Medeiros, R., 2012, *ApJ*, in prep. (LBLM12)

Ossenkopf, V., 2002, *A&A*, 391, 295

Padoan, P., Nordlund, A., & Jones, B. J. T. 1997, *MNRAS*, 288, 145

Padoan *et al.*, 2003, *ApJ*, 588, 881

Peek *et al.*, 2011, *ApJS*, 194, 20

Price, D., Federrath, C., & Brunt, C., 2011, *ApJ*, 727

Rosolowsky *et al.*, 1999, *ApJ*, 524, 887

Schekochihin, A. A., Cowley, S. C., Dorland, W., Hammett, G. W., Howes, G. G., Quataert, E., & Tatsuno, T. 2009, *ApJS*, 182, 310

Stanimirovic, S. & Lazarian, A., *ApJ*, 551, L53 (2001)

Stanimirovic, S., Staveley-Smith, L., Dickey, J. M., Sault, R. J., & Snowden, S. L., *MNRAS*, 302, 417 (1999)

Stutzki, J., Bensch, F., Heithausen, A., Ossenkopf, V., & Zielinsky, M., *A&A*, 336, 697 (1998)

Toffelmire, B., Burkhart, B., & Lazarian, A., 2011, *ApJ*, 736, 60